JOURNAL OF AIRCRAFT
Vol. 39, No. 1, January–February 2002

Load and Control Effects on Crack Growth in Flexible Aircraft

Sibok Yu* and Brett Newman†
Old Dominion University, Norfolk, Virginia 23529

The fundamental leverage generated by load tailoring and flight control system feedback loops for reducing fatigue damage and enhancing long-term integrity of aircraft structural components is investigated. Nonlinear fatigue behavior indicates two significant factors that influence crack growth are overload magnitude ratio and application period. This behavior implies existence of nonintuitive optimal overload strength and frequency values that minimize crack growth. Such results have important implications for design of new control logic that exploits this nonlinear phenomenon to suppress crack growth and enhance structural life. A state-space crack growth model is briefly reviewed and linked to a flexible aircraft model. Long-term structural integrity predictions, and the influence feedback control and loading variations have on such predictions, are made with a set of simulations covering the operational life of the vehicle. A mix of open-loop and closed-loop cases with nominal and variable feedback gains, vehicle motions including nominal maneuvers with superimposed gusts, deterministic and stochastic overloads, and mean stress levels are considered. For an existing control architecture, individual feedback gains have substantial influence on crack growth. This result implies significant extension of structural life may be possible by control gain adjustment within an existing architecture. Maneuver overload strength and frequency also have significant influence. By tailoring the overload maneuver with additional control logic, this result also implies significant structural life enhancement may be possible.

Introduction

OVER the operational lifetime of both military and civil aircraft, structural components are exposed to hundreds of thousands of low-stress repetitive load cycles.[1,2] In addition to this nominal, once per flight stress profile, the aircraft structure may experience random, infrequent high-stress transients due to, for example, emergency collision avoidance maneuvers or flight through energetic weather conditions. State-of-the-art, high-volume industrial processing and manufacturing has not yet reached a level where micromaterial imperfections, such as cracks and debonded laminates, are sufficiently absent within new aircraft structures. Under the flight loading environment just described, these imperfections expand and grow leading to a weakened structural system. An important factor limiting long-term structural integrity is the onset of rapid crack growth rates. References 3 and 4 provide a summary of common practices and newer methodologies for modeling and predicting the fracture mechanics of such systems.

As an airframe fleet approaches the end of its useful structural life, two options available for continuing operations include refurbishment of critical load-bearing components or altogether reinventorying the fleet with newer models. Neither option is very attractive, and alternative solutions for life extension of the airframe structure are, thus, highly desirable. One area having significant potential for impacting fatigue damage reduction is flight control. Feedback loops are routinely applied to vehicles to elicit desired motion characteristics. In principle, these same control loops can be utilized to influence exposure to harmful loads during flight. References 5 and 6 describe common load alleviation flight control systems that perform such functions.

Fatigue behavior predicted by experiment and simulation reveals two significant factors that influence crack growth: overload magnitude ratio and application period. This behavior leads to the existence of nonintuitive optimal overload strength and frequency values that minimize crack growth. Specifically, minimal crack growth and minimal overload strength are not synonymous due to nonlinear fatigue retardation and acceleration effects.[3,4] However, maneuver and gust load alleviation control systems are designed exclusively to perform load reduction. These observations have important implications for the design of new control logic that exploits nonlinear phenomena to suppress crack growth and enhance structural life. Such flight control systems could be thought of as generalized load alleviation systems, that is, maneuver and gust load-tailoring systems. Objectives of this research are to investigate the basic leverage generated by load tailoring and control system feedback for reducing fatigue damage and enhancing long-term structural integrity, and, thus, indirectly assess the potential benefit from a hypothetical load-tailoring flight control system.[7,8]

In this paper, a state-space crack growth model is briefly reviewed. Insight into nonlinear crack growth behavior is highlighted. Next, integration of a structural component stress model into an existing high-speed flexible aircraft transport model[9] is considered. The vehicle stress responses serve as input to the crack model. Vehicle dynamic traits are assessed, and the necessity for control augmentation is noted. Design of an integrated stability augmentation and structural mode suppression flight control system is considered. To address long-term structural integrity effects, simulations covering the operational life of the vehicle are made. A mix of open-loop and closed-loop cases with nominal and variable feedback gains, and with various excitations, are considered. Output data are used to project long-term structural integrity and to expose important factors influencing such integrity. These results are used to infer the potential leverage offered by a hypothetical generalized load-tailoring system designed to exploit nonlinear crack growth phenomena for enhanced structural life.

Crack Growth Model

The crack growth model used here originates from Refs. 10–12. Figure 1 shows a typical structural component that is associated with the crack model. The specimen is a notched thin rectangular plate. The plate is symmetric and axially loaded. Parameters describing the plate geometry include the half-width W, thickness t, notch half-width a_N, and notch height h_N. The far-field stress loading is σ. Figure 1 indicates the presence of cracks near both ends of the notch. The crack length (one side only) is denoted by C.

Received 1 May 2000; present as Paper 2000-4258 at the AIAA Guidance, Navigation, and Control Conference and Exhibit, Denver, CO, 14–17 August 2000; revision received 4 April 2001; accepted for publication 11 April 2001.

*Ph.D. Candidate, Department of Aerospace Engineering. Student Member AIAA.

†Associate Professor, Department of Aerospace Engineering. Senior Member AIAA.

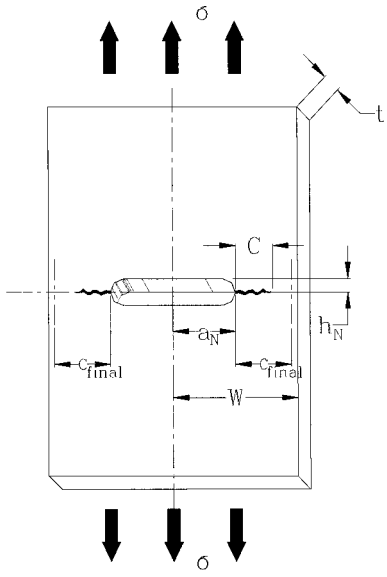

Fig. 1 Structural component specimen.

The analytical model describing specimen crack growth is

$$\frac{dC}{dN} = C_1\left\{F(\sigma_{max} - \sigma_0)\sqrt{\pi C}\right\}^m \qquad \text{for} \qquad \sigma_{max} \geq \sigma_0 \tag{1}$$

$$\frac{dC}{dN} = 0 \qquad \text{for} \qquad \sigma_{max} < \sigma_0 \tag{2}$$

where

$$F = \{\cos[(\pi/2)(C/W)]\}^{-\frac{1}{2}} \tag{3}$$

$$\sigma_0 = f(\sigma_{max}, \sigma_{min}, C) \tag{4}$$

In Eqs. (1–4), N is number of load cycles, σ_{max} (σ_{min}) is maximum (minimum) stress during the load cycle, σ_0 is crack opening stress, and F is a boundary condition correction factor. The parameters C_1 and m are positive constants identified from experiment. The nonlinear functionality in Eq. (4) is given fully in Ref. 8. The crack model is nothing more than a first-order differential equation for C in terms of N, where dC/dN represents the rate of crack growth. If crack growth is interpreted as a dynamic system, then Eqs. (1–4) are simply a state-space realization of this system. The model indicates crack growth rate is always nonnegative and, hence, crack length is a monotonically increasing function. The crack model is also highly nonlinear. In Eqs. (1) and (2), the factor $\sigma_{max} - \sigma_0$ plays the role of an input to the dynamic system. During any load cycle where $\sigma_{max} > \sigma_0$, the crack will have positive growth rate. If the difference between σ_{max} and σ_0 remains constant, then crack length will tend to increase with a power relationship ($\sqrt{C^m}$) as N increases. On the other hand, if σ_{max} falls below σ_0, then no growth occurs. Finally, with $\sigma_0 = 0$, Eqs. (1) and (2) indicate that for tension loading ($\sigma_{max} > 0$), positive growth rate occurs, but for compression loading ($\sigma_{max} < 0$), the growth rate is zero.

This system can exhibit both crack acceleration and retardation behavior. During cyclic loading, application of an isolated overload leads to a rapid increase in growth rate through the term $\sigma_{max} - \sigma_0$ in Eq. (1). Crack growth accelerates as excess material near the crack tip becomes plastic. Immediately following this event, the crack opening stress value σ_0 rises sharply as σ_{max} falls off to its nominal level. Through Eq. (2), a zero growth rate ensues. Growth rate is retarded because the postoverload condition is not sufficient to open the crack fully due to the presence of excess plastic material. As the specimen is further loaded, the crack opening stress value gradually reduces until it falls below the σ_{max} threshold. At this point, a positive growth rate returns as the material near the crack tip is once again fully loaded. This nonlinear behavior is counterintuitive and leads to an optimum overload corresponding to minimal crack growth.

Flexible Aircraft Model

A class of vehicles that may be particularly susceptible to excessive crack growth and fatigue damage is high-speed flexible transports. Consider such a vehicle with slender wing–body combination, conventional aft tail, and small forward canards. A complete nonlinear modeling effort for such a vehicle exists, and the development of low-order linear models for control synthesis is considered in Ref. 9. A linear 12th-order state space realization for a Mach 0.6 and 5000-ft altitude flight condition is given in Ref. 8. This model governs the coupled, small perturbation longitudinal rigid-body and structural vibration dynamics with

$$\dot{X}(t) = AX(t) + BU(t), \qquad Y(t) = CX(t) + DU(t) \tag{5}$$

where

$$X = [u \quad \alpha \quad \theta \quad q \quad \eta_i \quad \dot{\eta}_i]^T, \qquad (i = 1, 2, 3, 4)$$

$$Y = [q_{an1} \quad q_{cp} \quad a_{zcp} \quad \sigma_{cp}]^T, \qquad U = [\delta_e \quad \delta_c \quad \alpha_g]^T \tag{6}$$

In Eq. (6), state variables include forward speed u, angle of attack α, pitch angle θ, pitch rate q, and generalized structural deflection for the ith mode η_i and its rate $\dot{\eta}_i$. Four aeroelastic modes are included in the model. Inputs available for control include the elevator and canard deflections δ_e and δ_c, respectively, and α_g is a gust angle-of-attack disturbance. Responses of interest include pitch rate measured at two locations near the mode l antinode (approximate mass center) q_{an1} and near the cockpit q_{cp}, normal acceleration near the cockpit a_{zcp}, and stress near the cockpit σ_{cp}.

As the airframe undergoes longitudinal bending, fuselage stringers are axially loaded similarly to the generic material specimen described in Fig. 1. For a long slender flexible fuselage, forward stations such as the cockpit location will exhibit particularly high stress. Thus, stress associated with a longitudinal fuselage stringer at this location, σ_{cp}, was selected as an output of interest. This stress output was not an original component of the flexible vehicle model in Ref. 9 and, thus, required separate development. This development was based on an equivalent moment arm procedure using classic bending theory and the vehicle deflection mode shapes.[8] The stress output relationship in terms of vehicle states is

$$\sigma_{cp} = -Eh_e \sum_{i=1}^{4} \frac{d^2\phi_i}{dx^2}\eta_i \tag{7}$$

where ϕ_i is the ith mode shape, x is the coordinate along the fuselage centerline, E is the modulus of elasticity, and h_e is the equivalent moment arm. The nonzero elements in the vehicle C matrix corresponding to σ_{cp} are, thus, $-Eh_e d^2\phi_i/dx^2$. With such a relationship, the vehicle transient stress response due to maneuver and gust excitations is available for input to the crack growth model. Numerical values for all parameters in Eqs. (1–7) are given in Refs. 7 and 8.

Figures 2 and 3 show the open-loop vehicle frequency responses for measured pitch rates due to elevator input. One notable undesirable feature is the level of damping in the short-period

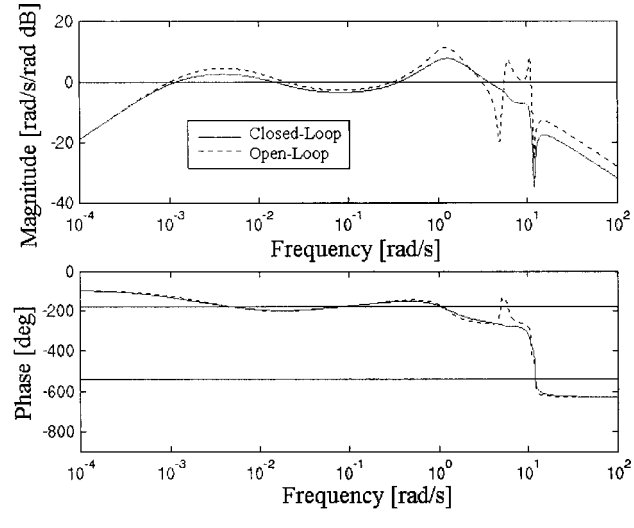

Fig. 2 Frequency response for $q_{an\,1}$, maneuver input.

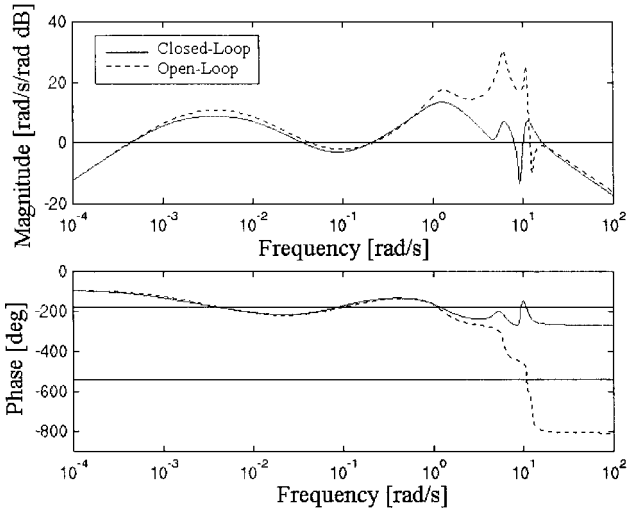

Fig. 3 Frequency response for q_{cp}, maneuver input.

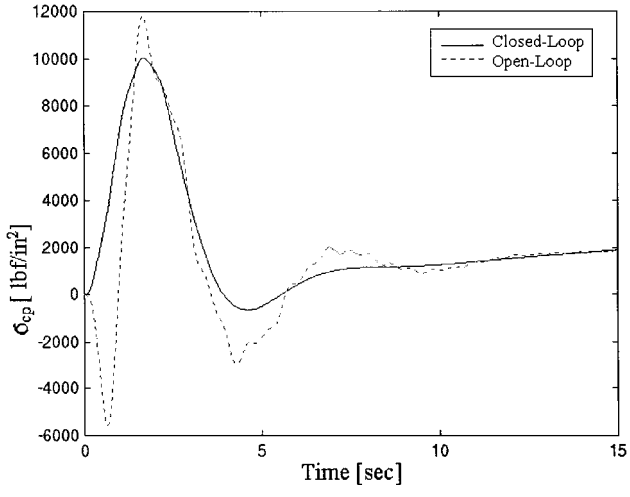

Fig. 4 Time response for σ_{cp}, maneuver input.

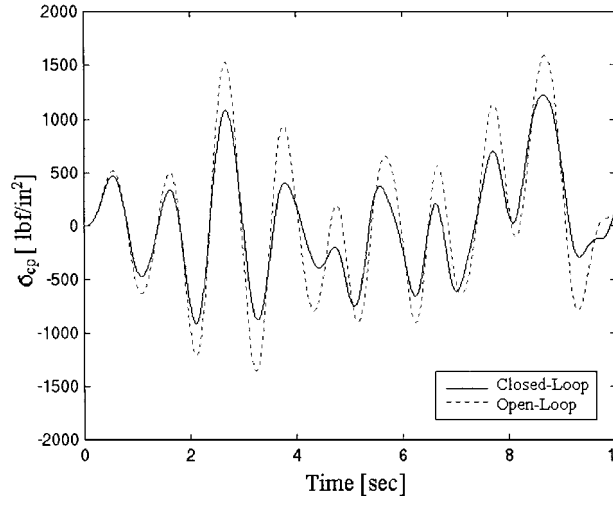

Fig. 5 Time response for σ_{cp}, gust input.

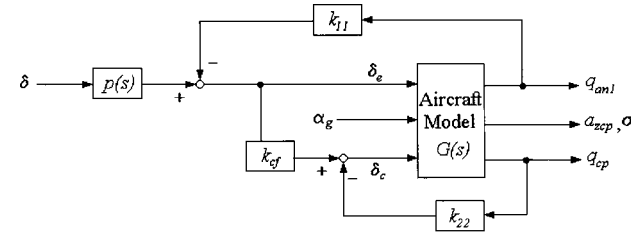

Fig. 6 Closed-loop system.

and aeroelastic modes. Short-period damping is $\zeta_{sp} = 0.36$ and first aeroelastic mode damping is $\zeta_{ae1} = 0.073$. In Figs. 2 and 3, this low damping corresponds to the sharp modal peaks occurring near 1 and 6 rad/s. Another deficiency in the airframe dynamics is the large aeroelastic modal contributions to the vehicle responses. In Figs. 2 and 3, the aeroelastic mode participation in the measured pitch rate transfer functions is on the order of or larger than the short-period participation. Finally, note the rapid 180-deg phase loss in Fig. 3 near 6 rad/s. This phase loss indicates a nonminimum phase behavior in the q_{cp}/δ_e transfer function. The nonminimum phase behavior is due to the noncollocated elevator and cockpit pitch rate actuator–sensor pair. These characteristics are unacceptable for manual control by a pilot and assistance from a flight control system is necessary.

Figure 4 shows the open-loop stress response at the cockpit due to a +1-deg filtered pulse input at the elevator applied for a duration of 1 s. The filter is first-order low pass with break frequency at 4 rad/s and approximates the neuromuscular limitations of the pilot. The transient stress response shows oscillatory behavior at multiple frequencies, including the short-period and first aeroelastic mode natural frequencies. The stress reaches a maximum value of 12,000 lbf/in.^{2} tension and approaches a steady value of near 2,000 lbf/in.^{2} tension after 15 s of motion as the vehicle comes to rest at its new attitude and deflection state. Note the stress values shown in Fig. 4 are only perturbation values from the mean stress state present at the original equilibrium point, possibly due to static trim deformation or fuselage pressurization, for example. To obtain the total stress, the mean value must be added to those in Fig. 4. Figure 5 shows the open-loop cockpit stress response due to a Dryden gust input with 1-ft/s gust standard deviation, 658.2-ft/s total flight velocity, and 2500-ft characteristic height. The stress standard deviation and statistical peak values based on a 100-s window are 630 lbf/in.^{2} and 1900 lbf/in.^{2} Structural components exposed to cyclic loading as in Figs. 4 and 5 would be compromised due to accelerated fatigue damage.

Control System Design

Objectives of the flight control system design are to correct the inherent deficiencies associated with the handling and ride characteristics noted earlier. These objectives include augmentation of the short-period and aeroelastic mode damping and suppression of aeroelastic contributions in the vehicle responses. Reduction of crack growth through direct augmentation of stress is not a primary objective. A conventional design approach consisting of sequential single-loop closures is utilized. The closed-loop architecture is given in Fig. 6, where $G(s)$ is the vehicle transfer matrix corresponding to Eq. (5), k_{11}, k_{22}, and k_{cf} are control gains, $p(s)$ is a dynamic prefilter, and δ is pilot stick input. The q_{cp} to δ_c loop is closed to improve the aeroelastic mode damping, especially for the first mode. A δ_e–δ_c crossfeed is applied to reduce aeroelastic motion excitation from the elevator. The q_{an1} to δ_e loop is closed to improve short-period damping. These three sequential design steps lead to the architecture in Fig. 6. The dynamic prefilter serves to lessen the trade between short-period damping augmentation and aeroelastic mode 2 destabilization associated with the k_{11} loop. Details of the design process and all numerical values in Fig. 6 may be found in Ref. 8.

Figures 2 and 3 also show the closed-loop frequency responses for the augmented vehicle. Note in Figs. 2 and 3 the closed-loop response has been scaled so that it matches the open-loop response at low frequency. Short-period damping has improved from $\zeta_{sp} = 0.36$ to $\zeta_{sp} = 0.55$, whereas the first aeroelastic mode damping has improved from $\zeta_{ae1} = 0.073$ to 0.14. These improvements are shown as reduced sharpness and height of the closed-loop short-period and first aeroelastic mode peaks in Figs. 2 and 3, relative to the open-loop traces. In addition to improved damping, the aeroelastic mode peaks and valleys located near $6 \sim 15$ rad/s in Figs. 2 and 3 are significantly reduced when compared to the corresponding open-loop behavior. This feature is a result of careful crossfeed and prefilter

augmentation. The first aeroelastic mode has been rendered less disturbable from pilot input, and the contamination of the vehicle responses by the aeroelastic modes is reduced relative to the open-loop system. Also note the phase loss in Fig. 3 has been reversed with control augmentation.

Another assessment of the closed-loop system concerns stability margins. Breaking the loop at δ_e and δ_c individually in Fig. 6 leads to the following upper gain margin (GM) and phase margin (PM) values:

$$\mathrm{GM}^{u}_{\delta_e} = 18.18\ \mathrm{dB}, \qquad \mathrm{PM}_{\delta_c} = \pm 163.64\ \mathrm{deg} \tag{8}$$

The stability margins are quite good and would satisfy most design requirements. This stability robustness superiority is inherent to the chosen feedback loops in Fig. 6. The numerical values indicate the q_{cp}/δ_c loop could be further tightened for increased damping of mode 1 with little risk of instability as measured by PM. Also, the $q_{\mathrm{an1}}/\delta_e$ loop can be tightened for further short-period damping augmentation. However, aeroelastic mode 2 limits the available bandwidth in this loop. Fortunately, short-period damping is sufficient. Note these margins are optimistic to some degree because the dynamic model assumes ideal actuators and sensors are available. Utilization of realistic models for the actuators and sensors would degrade the values listed in Eq. (8) somewhat. However, this added complexity was not considered essential to the research objectives and were, thus, neglected.

Even though control system objectives did not address stress response augmentation, the feedback loops in Fig. 6 impact these responses. Figure 4 also shows the closed-loop stress response at the cockpit due to a +1-deg filtered $[4/(s+4)]$ pulse input from the pilot command δ applied for a duration of 1 s. Note that in Fig. 4 the closed-loop response has been scaled so that it matches the steady-state open-loop response value. The closed-loop response is improved. The initial compressive peak in the open-loop response is eliminated, as well as high-frequency small-amplitude stress oscillations. The remaining dominant oscillatory peaks are about 20% less for the closed-loop system, relative to the open-loop system. The stress is responding primarily to the rigid-body pitch motion of the vehicle in the closed-loop case. The closed-loop cockpit stress response due to a unit Dryden gust is also shown in Fig. 5. The closed-loop stress standard deviation based on a 100-s window is 500 lbf/in.^{2} and is below the corresponding open-loop value (630 lbf/in.^{2}) indicating a reduced structural loading. The closed-loop stress peaks are reduced significantly when compared with the open-loop peak amplitudes. In summary, even though the flight control system was not specifically designed to influence the stress transients, the control loops do have a significant and beneficial effect on these transients. In the next section, these effects on crack growth and structural life will be explored.

Flight Profile Development

To investigate the influence feedback control and loading characteristics have on crack growth and long-term structural integrity, a matrix of test cases is considered in Table 1. Five loading cases are considered and include nominal profiles without and with gust and perturbed profiles with mean stress, maneuver overload, and gust overload. Nominal profile refers to the baseline maneuvers conducted during one single flight, and repeated over and over, to represent the operational usage during the structural life. Perturbed profiles are obtained by the indicated variation applied to the nominal profile. Table 1 also indicates three aircraft systems are considered and include nominal open-loop, nominal closed-loop, and perturbed closed-loop cases. The perturbed closed-loop case is generated by feedback gain variations. Simulation results indicated in Table 1 will allow crack growth comparisons to be made between open-loop and closed-loop behavior, between nominal closed-loop and gain varied closed-loop behavior, and between nominal flight loading and perturbed flight loading behavior. Before discussing these cases, nominal and perturbed flight profile development is necessary.

An isolated pitch maneuver initiated by pilot stick input, such as a pitch down-descend-pitchup sequence to decrease altitude, can be generated by a +1-deg pulse at the stick input applied for a duration of 1 s, followed by a −1-deg pulse initiated after 15 s of motion and also applied for a duration of 1 s. Note the stick input is again filtered to represent the limitations of the human neuromuscular system. The cockpit stress response for such an input applied to the open-loop flexible aircraft model is shown in Fig. 7. The pitch maneuver leads

Table 1 Simulation test cases

	System		
Loading	Nominal open loop	Nominal closed loop	Perturbed closed loop
Nominal profile	×[a]	×	×
Nominal profile, gust	×	×	
Perturbed profile,			
Maneuver overload	×	×	
Gust overload		×	
Mean stress		×	

[a] ×: Investigated test case.

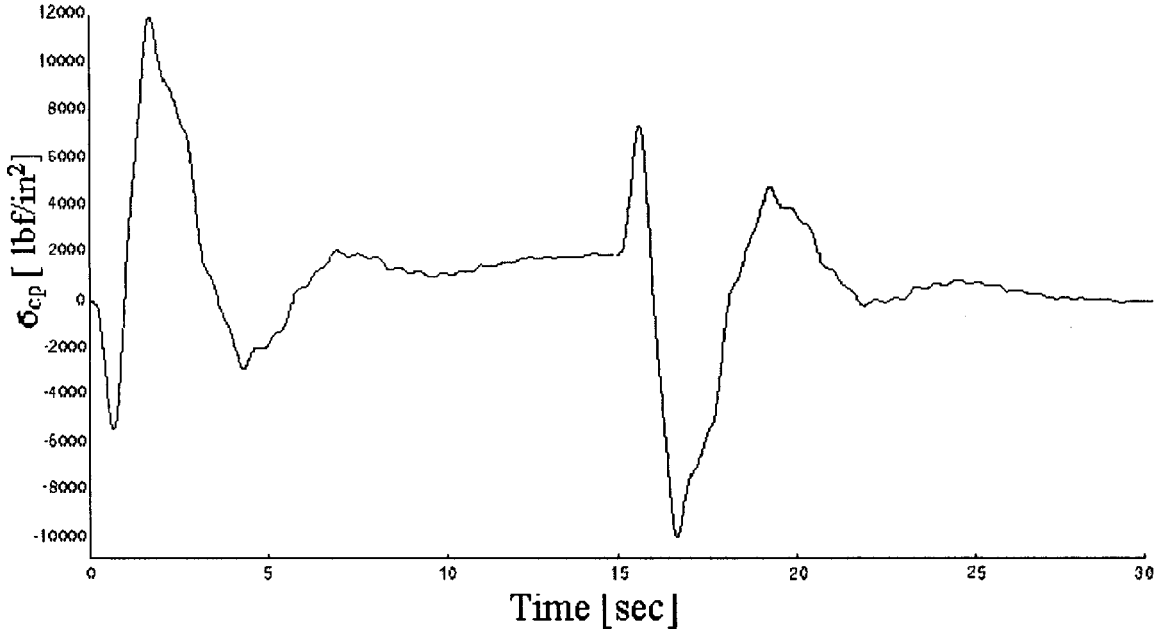

Fig. 7 Cockpit stress response for isolated pitch maneuver input.

to an initial transient stress response (pitch down), which settles to a steady value at 15 s (descend) and then undergoes another transient response (pitch up) before decaying back to the original zero value at 30 s (level flight).

A single operational flight is specified here to be a consecutive sequence of 10 isolated pitch maneuvers. This maneuver sequence and resulting nominal flight corresponds to the nominal profile load case in Table 1. The nominal profile with gust case in Table 1 is generated from the nominal flight profile by appending the stress response resulting from a unit Dryden gust with duration of 100 s after every flight. Note distinction between ascent and descent maneuvers was judged to be unimportant at this level of modeling. The perturbed profile with maneuver overload or gust overload cases in Table 1 are obtained from a variation of the nominal flight profile. In the maneuver case, after a specified number of nominal flights, N_1, the 10th and last pitch maneuver is amplified to represent a maneuver overload. The amplification factor is given by δ_2/δ_1, where δ_1 corresponds to the nominal stick input and δ_2 corresponds to an enlarged stick input. In the gust case, a Dryden gust input with duration of 100 s is applied. Here, the amplification factor is denoted by α_{g2}/α_{g1} with similar definition as earlier. These sequences are repeated over and over. The perturbed profile with mean stress case in Table 1 is obtained by simply adding a mean stress level to the nominal profile case.

To calibrate the temporal scale in subsequent aircraft structural life predictions, actual operational flight time and the vehicle age must be related to number of flights. A typical long-range transport averages about 6.67 h/flight. Moreover, about 600 flights are accumulated annually for such a transport. Therefore, excitation by 600 sets of the nominal flight profile is assumed to correspond to 4000 h of flight time or an approximate age of 1 year (600 flights $\approx$ 4000-h flight $\approx$ 1 year). Consider an example, which is helpful in understanding results in the remaining sections of this paper. If a vehicle structure was designed for 100,000-h flight, then this rating is equivalent to 100,000-h flight/6.67-h flight/flight $\approx$ 15,000 flights or 15,000 flights/600 flights/year $\approx$ 25 years. Assuming that 50% of the structural life was spent during crack initiation,[1] the number of flights corresponding to the period of measurable crack growth, and that which would be predicted by use of the crack growth model, is on the order of 7500 flights. Note the timescale in Fig. 7 (10×30 s) and a single flight (6.67 h) are not directly related because the aircraft may spend considerable periods of time in a steady climb or descent, or in cruise. This observation does not affect the results, however, because stress is constant during these flight conditions.

Two additional comments are made before considering the simulation results. The crack growth model in Eqs. (1–4) is excited by a discrete input. Thus, intermediate points lying between peak values in Fig. 7 have no effect on crack growth. Peak values are, thus, extracted from the vehicle stress response before application to the crack model. Also for the assumed crack growth model, negative or compressive stress has no influence on crack growth [see Eqs. (1–4)]. Thus, all negative stress data points are set to zero before being inputted to the crack growth model. Simulation results for each of the load cases in Table 1 are discussed next.

Nominal Profile and Control

In this section, a comparison is made between the crack growth behavior associated with the open-loop vehicle and closed-loop vehicle when excited by the nominal flight profile and the nominal flight profile with gust. Figure 8 shows crack growth length vs number of flights corresponding to the preceding four cases. Starting from an initial crack length of 12.7 mm, in all cases the crack growth follows a power relationship. The stress loading is applied until the crack length reaches a specified limit of 40 mm. The theoretical upper bound for this value (in this application) is the half-width $W = 76.2$ mm. The specified value is roughly 50% of this upper bound and provides a reasonable threshold where the structural member is judged to be ineffective in supporting load.

For the open-loop vehicle excited by the nominal flight profile with and without gust, observe the crack length in both cases reaches the specified upper limit of 40 mm after approximately 1700 flights.

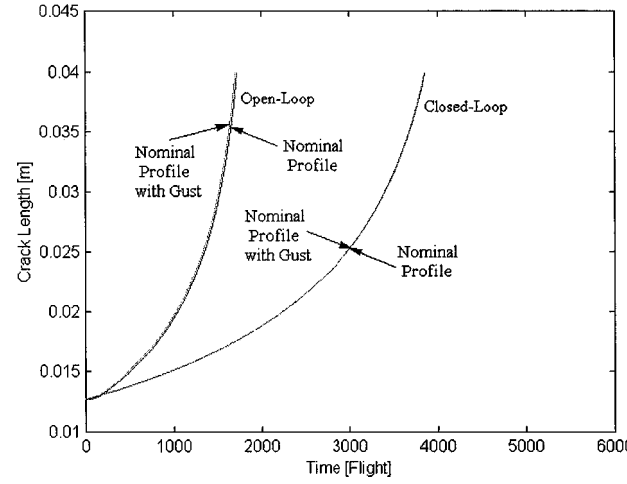

Fig. 8 Crack growth comparison for nominal flight profiles.

The presence of additional loading on the vehicle structure due to the gust results in a small and insignificant decrease in structural integrity (increased crack growth rate). For the closed-loop vehicle excited by the same load cases, similar behavior is observed. The presence of the nominal gust in each flight has little or no impact on structural integrity.

For the closed-loop vehicle excited by the nominal flight profile with and without gust, note that the crack length reaches 40 mm after approximately 3860 flights. Based on the result in Fig. 8, significant extension of structural life is predicted when there is utilization of a flight control system. Closed-loop structural life is more than double (approximately 130%) the value for the open-loop case. Based on the temporal calibration given earlier, an enhancement of structural life by 2160 flights corresponds to an additional 14,400 h flight service or an increment in usable vehicle age of 3.6 years.

Recall that the indicated number of flights from Fig. 8 must be supplemented with usage required to initiate a crack dimension of 12.7 mm, and this usage can be up to 50% of the total life.[1] This additional factor of 2 is not included in the preceding comparisons. Thus, the projections could be as high as 28,800-h flight or 7.2 years. Also understand that these projections are based on an arbitrary final crack length of 40 mm, which is inherently tied to the specific geometry considered in Fig. 1. As a final caveat, the open-loop vehicle is very flexible and most likely is not intended for operation without feedback loops. Thus, structural life projections based on comparison to the open-loop vehicle may be optimistic, in some sense.

Feedback Gain Variation

The effect of control gain variations on structural life is investigated in this section. Recall the control gains k_{22}, k_{cf}, and k_{11} from the control system in Fig. 6. Note that primary functions of these gains were to augment aeroelastic damping, to reduce aeroelastic excitation from pitch inputs, and to augment short-period damping, respectively. Figure 9 shows crack length vs number of flights for a family of k_{22} values. The open-loop behavior is also included for comparison. Here k_{22} is varied from 0.03 to 0.075 rad/rad/s with increments of 0.005 rad/rad/s. Note the nominal gain value is $k_{22} = 0.05$ rad/rad/s.

For feedback gain values of 0.05 and 0.075 rad/rad/s, the crack length attains a value of 40 mm in 3860 and 4580 flights, respectively. The results show that increased gain values for k_{22} correspond to substantial extended structural life. A 50% gain increase ($k_{22} = 0.075$ rad/rad/s) from the nominal value for k_{22} yields a projected 19% enhancement to the structural life. This 19% enhancement is equivalent to a service of 4800-h flight and an age of 1.2 years. Again, these projections could increase by a factor of 2 when accounting for the crack initiation phase of the total structural life.

Figures 10 and 11 show the crack length vs number of flight characteristics for families of k_{cf} and k_{11} values. The gain k_{cf} is varied

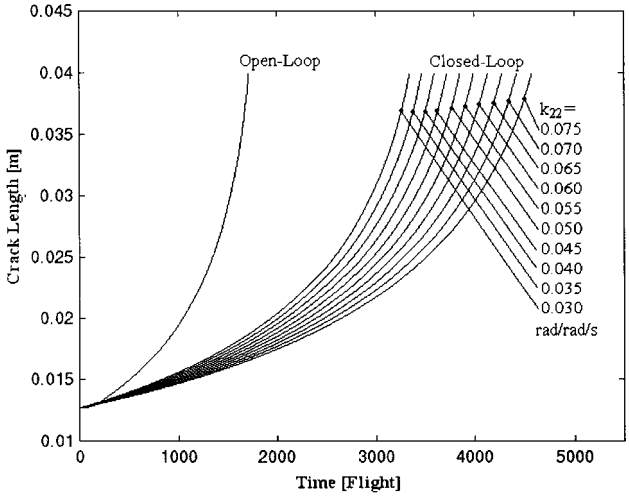

Fig. 9 Crack growth behavior, variable k_{22}.

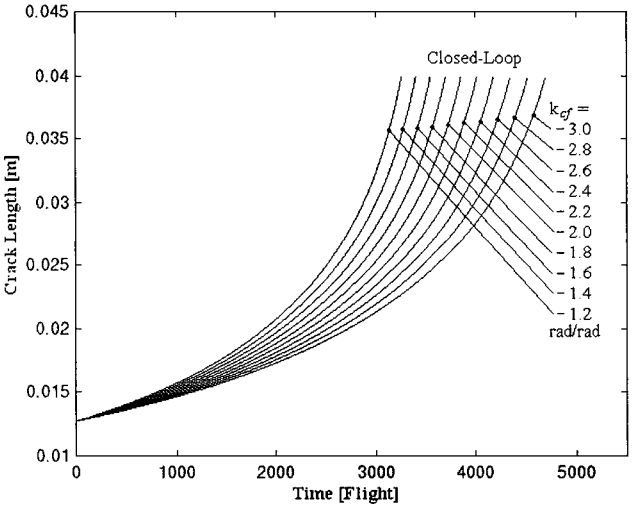

Fig. 10 Crack growth behavior, variable k_{cf}.

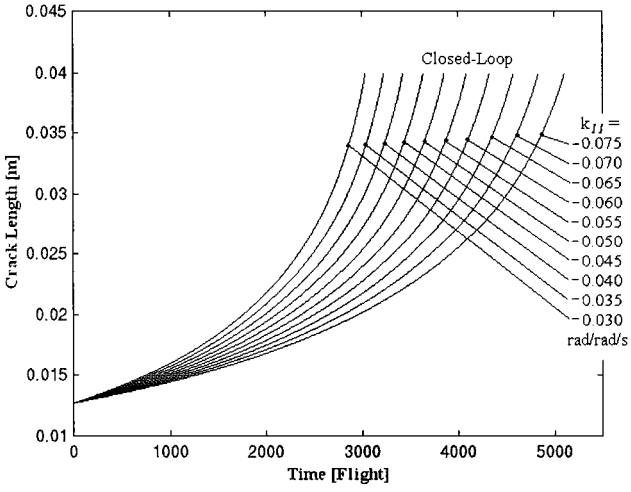

Fig. 11 Crack growth behavior, variable k_{11}.

from -1.2 to -3 rad/rad by increments of 0.2 rad/rad, whereas for k_{11}, the range is from -0.03 to -0.075 rad/rad/s with increments of 0.005 rad/rad/s. Note that the nominal gain values are $k_{cf} = -2$ rad/rad and $k_{11} = -0.05$ rad/rad/s. Results imply increased gain (or the absolute value of gain) for either k_{11} or k_{cf} will lead to extended life. Gain variations corresponding to 50% increments ($k_{cf} = -3$ rad/rad and $k_{11} = -0.075$ rad/rad/s) from the nominal level yield additional numbers of flight on the order of 840 flights and 1250 flights, respectively. For k_{cf}, 840 flights correspond to 5600-h flight or 1.4 years. For k_{11}, 1250 flights is equivalent to 8333-h flight or 2.1 years.

In all gain variation cases, tighter feedback loops provide more influence while controlling stress response levels and, hence, crack growth behavior. Gain k_{11} appears to have the most leverage on reducing crack growth. This observation is consistent with Fig. 4, where it was noted that the short-period mode provides the dominant contribution to the overall closed-loop stress response. Optimization of control gains is an attractive means for leveraging the structural life.

Vehicle Stability and Performance Trades

In the preceding section, the potential benefit on structural life enhancement from control system retuning was investigated. The investigation proceeded by adjusting control system parameters and observing the resulting crack growth behavior. Most likely, large gain adjustment outside some neighborhood surrounding the nominal values is infeasible without compromising some or all critical flight dynamic characteristics. In this section, trades between closed-loop vehicle stability and performance and vehicle structural life, while undergoing feedback gain variations, are explored and exposed.

As in the nominal case, the elevator loop upper GM and canard loop PM are dependent on the feedback gains, and these dependencies are shown in Figs. 12 and 13. Results in Fig. 12a indicate a significant trade exists between structural life and vehicle closed-loop stability. As the absolute value of k_{11} is enlarged to enhance

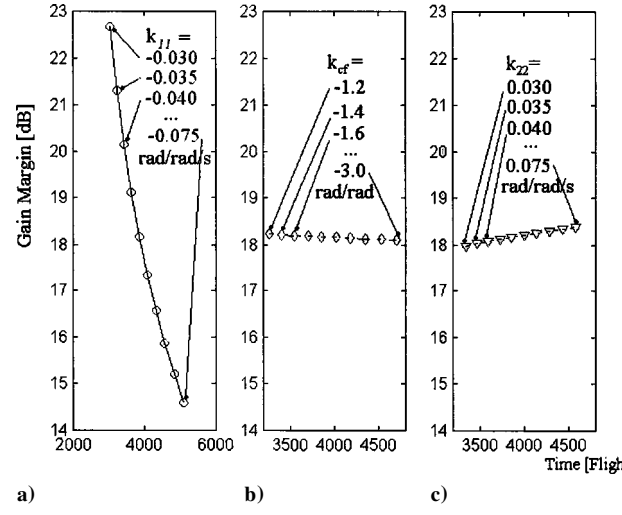

Fig. 12 Upper GM for δ_e vs structural life, variable k_{11}, k_{cf}, and k_{22}.

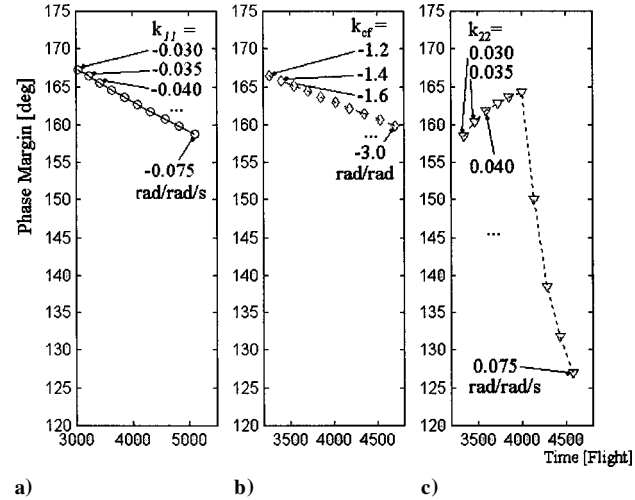

Fig. 13 PM for δ_e vs structural life, variable k_{11}, k_{cf}, and k_{22}.

structural life, the closeness to instability becomes smaller. For example, as the gain k_{11} increases from a nominal value of -0.05 to -0.075 rad/rad/s, the crack length attains a value of 40 mm in 3860 and 5110 flights, respectively. Simultaneously, the upper GM for the elevator loop decreases from 18.2 to 14.6 dB. These values give a GM to flight number sensitivity of -0.0029 dB/flight. Although the values for GM from Fig. 12a are quite high and the indicated losses would not pose any serious compromise to stability, the rate at which GM is traded off for enhanced structural life is significant. Recall that stability of aeroelastic mode 2 is the limiting factor here. Figures 12b and 12c show a weak dependency between GM and structural life. The elevator loop upper GM is nearly constant as the structural life is extended through enlargements of k_{cf} and k_{22}.

Figures 13a and 13b show that enlargement of k_{11} or k_{cf} results in a small to modest decrease in PM. On the other hand, Fig. 13c shows that both increased and decreased values for k_{22} decrease PM. Thus, the nominal system is at a near optimum condition for PM. When k_{22} is enlarged from 0.05 to 0.075 rad/rad/s, the crack length attains a value of 40 mm in 3860 and 4580 flights, respectively. Simultaneously, the PM decreases from $+164$ to $+127$ deg. These values give a PM to flight number sensitivity of -0.051 deg/flight. Again, although the preceding values for PM in Fig. 13 are quite high and the indicated losses would not pose any serious compromise to stability, the rate at which PM is traded off for enhanced structural life is significant. The limiting factor here is mode 1 itself.

Figures 14 and 15 show augmented short-period and aeroelastic mode 1 damping vs number of flights for the feedback gain variations conducted earlier. Results in Figs. 14a–14c indicate a small benefit

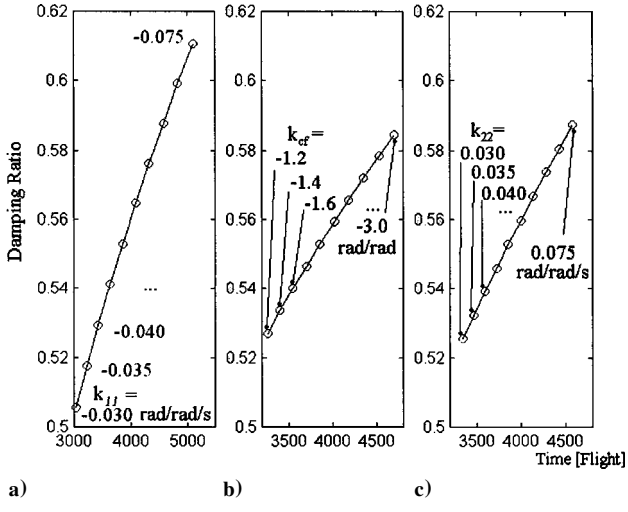

Fig. 14 Short-period damping ratio vs structural life, variable k_{11}, k_{cf}, and k_{22}.

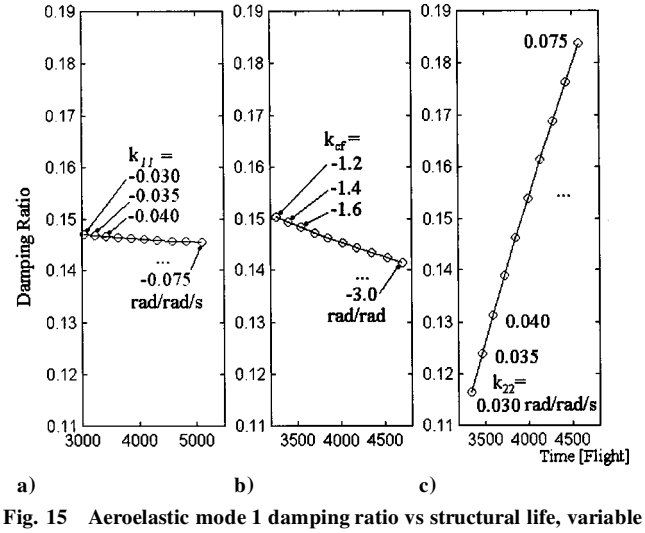

Fig. 15 Aeroelastic mode 1 damping ratio vs structural life, variable k_{11}, k_{cf}, and k_{22}.

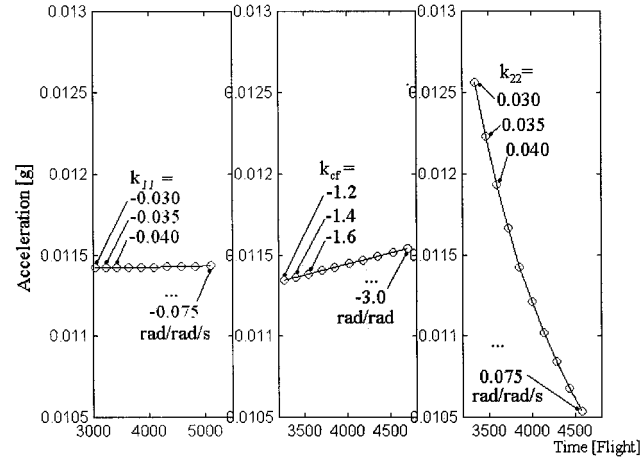

Fig. 16 Cockpit acceleration standard deviation vs structural life, variable k_{11}, k_{cf}, and k_{22}.

in closed-loop performance as measured by short-period damping as k_{11}, k_{cf}, and k_{22} are increased to achieve longer structural life. As an example, consider Fig. 14a. As the gain k_{11} increases from a nominal value of -0.05 to -0.075 rad/rad/s, the crack length attains a value of 40 mm in 3860 and 5110 flights, respectively. During this same gain change, augmented short-period damping increases from 0.553 to 0.611. These values give a short-period damping to flight number sensitivity of $+0.000046$ 1/flight. This level of performance sensitivity can be considered as small. Figures 14b and 14c show similar small benefits.

Data from Fig. 15c show a significant benefit in augmented aeroelastic mode 1 damping as k_{22} is increased to enhance structural life. As the gain k_{22} increases from a nominal value of 0.05 to 0.075 rad/rad/s, crack length reaches 40 mm in 3860 and 4580 flights, respectively. During this same gain variation, augmented aeroelastic mode 1 damping increases from 0.146 to 0.184. From these values, an aeroelastic mode damping to flight number sensitivity of $+0.000053$ 1/flight results. This sensitivity level is significant when considering the small damping levels that exist for mode 1. The results in Figs. 15a and 15b for k_{11} and k_{cf} show small damping tradeoffs as the structural life is extended. Trends in Figs. 14 and 15 are consistent with the primary roles of gains k_{11} and k_{22}.

Figure 16 shows cockpit acceleration standard deviation vs number of flights for the feedback gain variations considered in this research. Results indicate a moderate benefit in cockpit ride quality as k_{22} is increased to enhance structural life. As the gain k_{22} increases from a nominal value of 0.05 to 0.075 rad/rad/s, the crack length equals 40 mm after 3860 and 4580 flights, respectively. Under this same gain variation, the cockpit acceleration standard deviation varies from 0.0114 to 0.0105 g, respectively. These values yield a cockpit acceleration level to flight number sensitivity of -0.0000013 g/flight. Increased aeroelastic damping through gain variation leads to this moderate improvement in cockpit ride quality. Results for k_{11} and k_{cf} show nearly constant cockpit acceleration levels with gain variations. These results are consistent with Fig. 5, where cockpit stress is dominated by aeroelastic contributions.

Maneuver Overload

In this section, investigations concerning crack growth dependency on maneuver overload ratio and period are given. Figure 17 shows crack length vs number of flights for a range of overload ratio values for the open-loop vehicle. The overload ratio is varied from 1 to 4. Note that this overload ratio is synonymous with the scaling δ_2/δ_1 applied to the extreme pitch maneuver representing the maneuver overload. In generating Fig. 17, the overload period is held fixed at $N_1 = 10$ flights. Similar to experimental observations for test specimens,[4] the integrated flexible aircraft–crack model exhibits nonintuitive behavior. For the range $1 \leq \delta_2/\delta_1 \leq 1.8$, crack growth

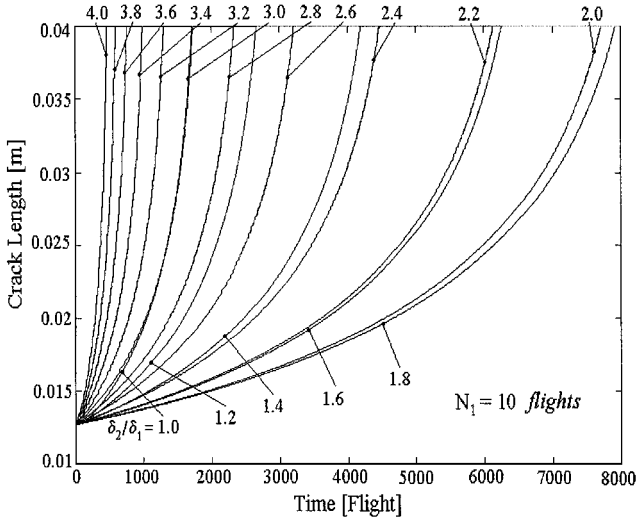

Fig. 17 Open-loop fatigue behavior, maneuver overload.

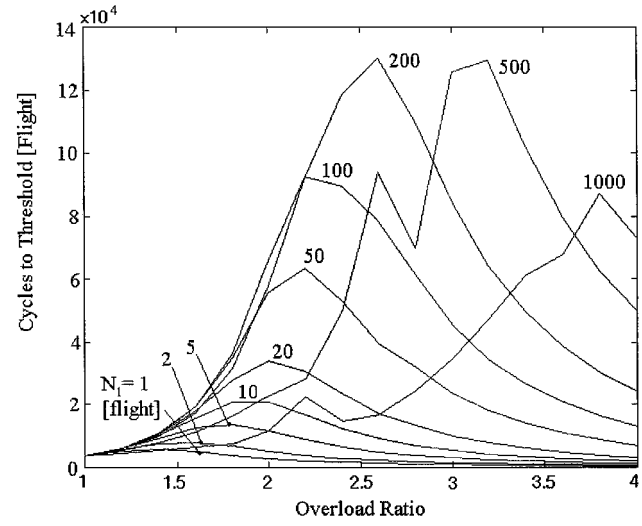

Fig. 19 Closed-loop cycles to threshold, maneuver overload.

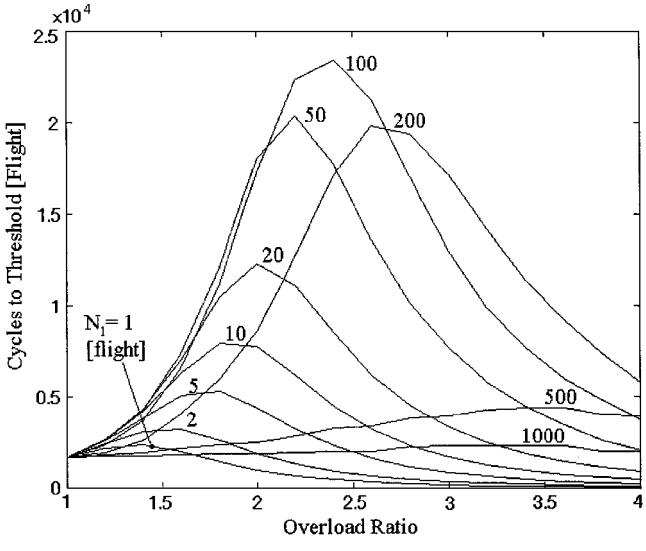

Fig. 18 Open-loop cycles to threshold, maneuver overload.

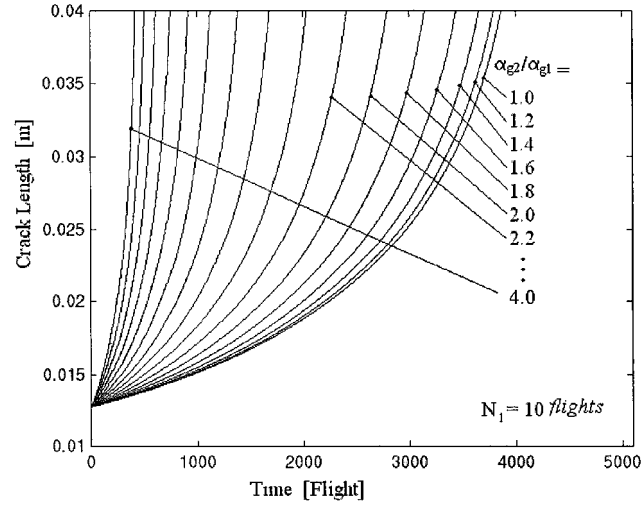

Fig. 20 Closed-loop fatigue behavior, gust overload.

rate decreases with strengthening overloads. On the other hand, for $2 \leq \delta_2/\delta_1 \leq 4$, the trend reverses, crack growth rate increases with increasing overload ratio. Nonintuitive fatigue behavior is clearly present and leads to an optimum overload ratio, which results in minimum fatigue damage. From Fig. 17, this optimum value is near 1.8.

The terminal points corresponding to 40 mm in Fig. 17 are used to construct the $N_1 = 10$ flight cycles to threshold summary chart in Fig. 18. This chart shows the available cycles until threshold (40 mm) and its dependency on overload ratio. The optimum overload ratio (for $N_1 = 10$ flights) is near 1.8. This optimum overload condition provides important implications for flight control redesign and exploitation. For example, suppose the aircraft structure in the vicinity of the crack experiences a maneuver overload of strength 1.25 or 2.6 with $N_1 = 10$ flights. If a flight control system were to readjust the maneuver execution corresponding to a strength of 1.8, and assuming this readjustment was done repeatedly, the result would be an increase in structural life of approximately 5000 flights. This value is equivalent to 33,333-h flight or 8.3 years in age.

Overload period can also have significant influence on the crack growth behavior. The earlier calculations for $N_1 = 10$ flights leading up to Fig. 18 are revisited with a range of values for N_1 with the open-loop vehicle. The overload period ranges from 1 to 1000 flights. Figure 18 shows these results for variable overload period. The optimum overload ratio shows dependency on the overload period. As the period increases (less frequent overload occurrences), the optimum overload ratio increases. For example, with $N_1 = 10$ vs 50 flights, the optimum ratio shifts from approximately 1.8 toward a value of 2.2. Figure 19 shows the corresponding cycles to threshold chart for the closed-loop vehicle. Similar behavior is observed, but the potential extensions to structural life are considerably higher. Note that for N_1 values above 200 flights, there appears to be multiple local optimum overload ratios.

Gust Overload

In this section, effects from overload ratio and overload period on crack growth behavior are again addressed. However, a distinctly different excitation source is considered here, that is, atmospheric gust. Figure 20 shows crack length vs number of flights for a range of overload ratio values for the closed-loop vehicle. The overload ratio is again varied from 1 to 4. This overload ratio is equivalent to the scaling α_{g2}/α_{g1} applied to the Dryden turbulence excitation representing the gust overload. Figure 20 corresponds to a fixed overload period of $N_1 = 10$ flights. In contrast to the maneuver overload behavior just presented, the results shown here exhibit monotonically increasing crack growth rate as the overload ratio increases. For the entire range $1 \leq \alpha_{g2}/\alpha_{g1} \leq 4$, crack growth increases as overload ratio increases. Here, minimal crack growth corresponds to minimal loading.

The cycles to threshold (40 mm) chart generated from Fig. 20 and corresponding to an overload period of 10 flights is given in Fig. 21. As the overload strength increases, the structural life steadily decreases in a nonlinear fashion. The implications for flight control redesign here are simply to reduce the structural loading in the vicinity

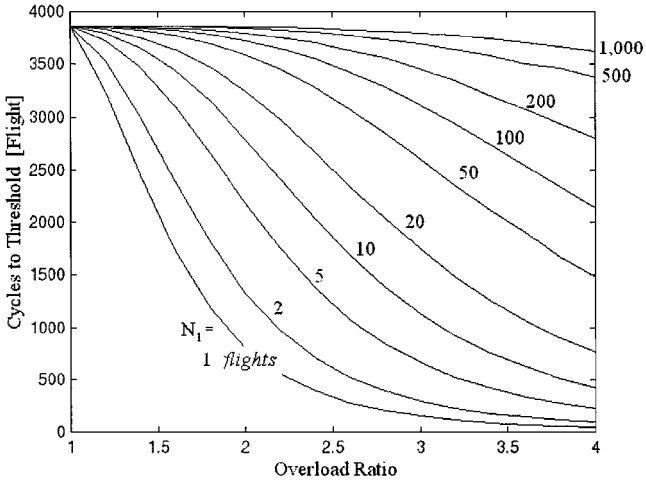

Fig. 21 Closed-loop cycles to threshold, gust overload.

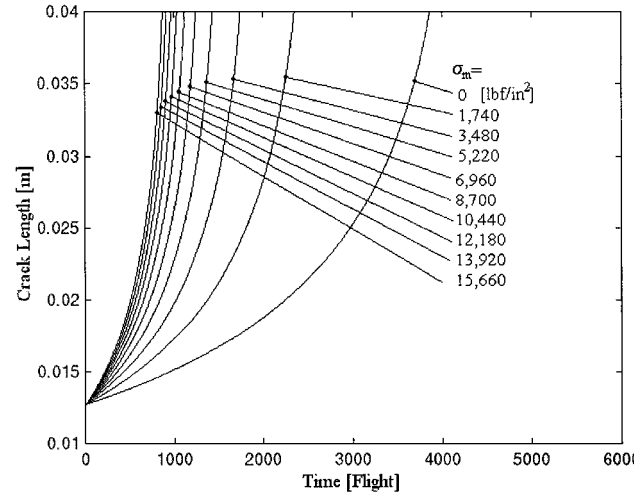

Fig. 22 Effect of mean stress on crack growth.

of a crack due to gust excitation. For example, if the structural loading due to gust can be reduced repeatedly from an overload ratio of 3 to 2 for $N_1 = 10$ flights, structural life can be extended by approximately 1700 flights. This extension corresponds to a service of 11,333-h flight or an age of 2.8 years.

The monotonically decreasing nature of the gust overload case shown in Fig. 21 is fundamentally distinct from the behavior displayed in Fig. 19 associated with maneuver overload. Recall the stress response corresponding to a pitch maneuver overload is an amplified response similar to that shown in Fig. 4. After eliminating compressive stresses, the response is primarily a single dominate stress peak with many smaller surrounding stress oscillations. Sequences of this loading structure are highly correlated to an input template with isolated overloads, which is known to result in crack retardation and acceleration behavior.[4] In contrast, the stress response corresponding to an atmospheric gust overload is an amplified response similar to that shown in Fig. 5. Here, the response consists of many equally dominant stress peaks and is not well correlated with common input templates. There is no single dominant stress peak. The conclusion is that a distributed overload like the gust overload does not elicit crack growth retardation behavior.

Figure 21 shows the cycles to threshold chart when both overload ratio and overload period are allowed to vary. As the period between gust overload occurrences increases (increasing N_1), the structural life also increases. Implications for flight control are again significant. For example, consider a gust overload scenario occurring at a ratio of 3 and period of 10 flights. Suppose an existing flight control logic set reduces every overload occurrence to a ratio of 2.5. The remaining structural life in this case is 1800 flights (see Fig. 21 at $\alpha_{g2}/\alpha_{g1} = 2.5$ and $N_1 = 10$ flights). Now consider another logic set that aggressively reduces four consecutive overload occurrences to a ratio of near 1 and leaves every fifth overload ratio at 2.5. In this case, the remaining structural life is 3200 flights (see Fig. 21 at $\alpha_{g2}/\alpha_{g1} = 2.5$ and $N_1 = 50$ flights). The new flight control logic set increases structural life by 1400 flights or 9333-h flight or 2.3 years.

Mean Stress

In this section, the effects of mean stress on structural life are investigated. The stress response coming from the flexible aircraft model, such as in Fig. 4, is only a perturbation from the mean stress state present at the original equilibrium point. Mean stress could originate from, for example, fuselage/cabin pressurization or fuselage deformation at trim. To obtain the total stress, the mean value is added to the perturbation value.

Figure 22 shows crack length vs number of flights corresponding to the preceding case. Mean stress σ_m is varied from 0 to 15,660 lbf/in.^{2} When starting from an initial crack length of 12.7 mm, in all cases the crack growth follows a power relationship. The stress loading is applied to the crackmodel until the crack length reaches the specified limit of 40 mm. Note that mean stress has a significant impact on the crack growth behavior. Increased mean stress yields higher crack growth rates. Furthermore, observe this relationship is highly nonlinear. For example, a 1740 lbf/in.^{2} change in mean stress occurring at 0 and at 1740 lbf/in.^{2} nominal conditions leads to significantly different growth rates. The growth rate sensitivity saturates at higher mean stress levels.

Conclusions

This research investigates the influence of feedback control, and other factors associated with loading characteristics, on fatigue damage reduction and long-term integrity of aircraft structural components. Computer simulations of a combined flexible aircraft and state-space crack model are utilized in the investigations. Simulation results point out several governing factors that have significant influence on crack growth. Critical governing factors include the nominal control system feedback loops, individual feedback gains of the control system, mean stress level, overload ratio, and overload period.

First, consider the factors associated with control. The presence of a nominal control system turned out to be very important. Results show that, for a flexible airframe, a nominal control system can double the structural life when compared to the airframe alone without control system. Another important factor is the control parameters. Individual feedback gain values of the control system can provide significant leverage for extending structural life. This conclusion implies potential life extension is attainable by simply adjusting control parameters of an existing flight control system.

Among the various feedback gains, k_{11} shows the most significant influence on structural life extension. With regard to closed-loop stability, k_{cf} and k_{22} show small impacts on GM whereas k_{11} shows a large undesirable influence on GM. Enlargements in k_{11} and k_{cf} decrease the PM by small amounts whereas k_{22} shows a large undesirable influence on PM. Concerning closed-loop performance, an enlargement of control gains k_{11}, k_{cf}, and k_{22} modestly increases the short-period mode damping. On the other hand, enlargement of k_{22} increases aeroelastic mode 1 damping sizably and improves cockpit ride quality considerably, whereas increased absolute values for k_{11} and k_{cf} decrease aeroelastic damping by a small amount and have little influence on cockpit ride quality. No single control gain can leverage structural life and avoid impacting closed-loop stability and performance.

Second, consider factors associated with the equilibrium stress state. Mean stress shows a large undesirable influence on structural life. If equilibrium structural deflection is a large contributor to mean stress, and if the vehicle has multiple control surfaces, it is conceivable to redistribute the control surface inputs to reduce structural deflection (and, hence, mean stress) while still maintaining the desired flight condition.

Third, consider factors associated with the loading. Excitation sequences applied to the vehicle structure that include maneuver-type

overloads have very significant influence on the structural life. Results indicate existence of nonintuitive optimal overload strength and optimal overload frequency conditions that minimize crack growth and maximize structural life. Specific cases exist where higher maneuver overloads actually reduce fatigue damage. These results have very significant implications for flight control. When any overload maneuver is tailored with appropriate flight control logic, large payoffs are projected for structural life. Optimizing overload strength and frequency can lead to large structural life enhancements in cases considered here. On the other hand, gust-type overloads applied to the vehicle simply decrease structural life. Gust overloads should be minimized by the flight control load-tailoring logic.

References

[1]Bruhn, E. F., *Analysis and Design of Flight Vehicle Structures*, Jacobs, Indianapolis, IN, 1973, Chap. 13, pp. C13.1–C13.49.

[2]Lomax, T. L., *Structural Loads Analysis for Commercial Transport Aircraft: Theory and Practice*, AIAA, Reston, VA, 1996, Chap. 2.

[3]Liebowitz, H., "Fracture Mechanics of Aircraft Structures," AGARD AG-176, Jan. 1974.

[4]Norman, E. D., *Mechanical Behavior of Materials*, Prentice–Hall, Upper Saddle River, NJ, 1999, Chaps. 8–11.

[5]Wykes, J. H., "Structural Dynamic Stability Augmentation and Gust Alleviation of Flexible Aircraft," AIAA Paper 68-1067, Oct. 1968.

[6]White, R. J., "Improving the Airplane Efficiency by Use of Wing Maneuver Load Alleviation," *Journal of Aircraft*, Vol. 8, No. 10, 1971, pp. 769–775.

[7]Yu, S., "Long-Term Aircraft Structural Integrity Prediction Under the Influence of Feedback Control," M.S. Thesis, Dept. of Aerospace Engineering, Old Dominion Univ., Norfolk, VA, Dec. 1999.

[8]Yu, S., and Newman, B., "Flight Control Leverage on Crack Growth in a Flexible Aircraft, Parts 1 and 2," AIAA Paper 2000-4257 (A00-37094), AIAA Paper 2000-4258 (A00-37095), Aug. 2000.

[9]Newman, B., and Schmidt, D. K., "Numerical and Literal Aeroelastic-Vehicle-Model Reduction for Feedback Control Synthesis," *Journal of Guidance, Control, and Dynamics*, Vol. 14, No. 5, 1991, pp. 943–953.

[10]Patankar, R., Ray, A., and Lakhtakia, A., "A State-Space Model of Fatigue Crack Growth," *International Journal of Fracture*, Vol. 90, No. 3, 1998, pp. 235–249.

[11]Newman, J. C., "A Crack Opening Stress Equation for Fatigue Crack Growth," *International Journal of Fracture*, Vol. 24, No. 4, 1984, pp. R131–R135.

[12]Newman, J. C., Phillips, E. P., and Everett, R. A., Jr., "Fatigue Life and Crack Growth Prediction Methodology," NASA TM-109044, Oct. 1993.